Front. Phys. China, 2010, 5(4): 347–356
DOI 10.1007/s11467-010-0104-9

MINI-REVIEW ARTICLE

# Synthesis and assembly of magnetic nanoparticles for information and energy storage applications

**Hong-wang ZHANG** (张洪旺), **Yi LIU** (刘毅), **Shou-heng SUN** (孙守恒)†

*Department of Chemistry, Brown University, Providence, Rhode Island 02912, USA*
*E-mail:* †*ssun@brown.edu*

*Received June 7, 2010; accepted June 21, 2010*

This mini-review summarizes the recent advances in chemical synthesis and assembly of monodisperse magnetic nanoparticles for magnetic applications. After a brief introduction to nanomagnetism, the review focuses on recent developments in solution phase syntheses and assemblies of monodisperse Fe, CoFe, FePt and $SmCo_5$ nanoparticles. The review further outlines the structural and magnetic properties of these nanoparticles for magnetic information and energy storage applications.

**Keywords** magnetic nanoparticle, self-assembly, data storage, energy storage

**PACS numbers** 75.75.-c, 75.75.Cd, 81.16.Be

Contents



## 1 Introduction

Bulk ferromagnetic (FM) materials contain multiple magnetic domains that respond to an external magnetic field *via* domain wall nucleation/movement and magnetization rotation [1, 2]. The single-domain size of a given material can be estimated by $R_{sd} = 36\sqrt{AK_u}/(\mu_0 M_s^2)$, where $A$ is the exchange constant, $K_u$ is the effective anisotropy constant and $M_s$ is the saturation magnetization [3]. For most magnetic materials, $R_{sd}$ falls in the range of 10–100 nm. However, it can also reach several hundred nanometers for materials with large $K_u$ [3].

When the physical dimension of an FM material is reduced to nanometer scale, the multi-domain structure cannot be supported and therefore, the material is often referred to as single domain FM nanoparticles (NPs). A group of single-domain magnetic NPs has the similar hysteresis loop of the corresponding bulk FM material, as shown in Fig. 1(a). Upon the application of an external magnetic field, the magnetization of these NPs can be aligned along the direction of the external field and be saturated to reach maximum magnetic moment ($M_s$). Subsequent reduction of field strength leads to certain degree of decrease in magnetic moment due to various magnetization relaxation processes. When the field strength drops back to zero, the magnetization of these NPs tends to retain the previous direction with a measureable remnant magnetic moment ($M_r$). To demagnetize these NPs so that they have zero overall magnetic moment, the external magnetic field must be applied in an opposite direction. The field strength required to demagnetize these NPs is defined as coercivity ($H_c$). By further increasing the strength of the reverse field, the magnetization of all NPs can be aligned along the opposite direction ($-M_s$) [1].

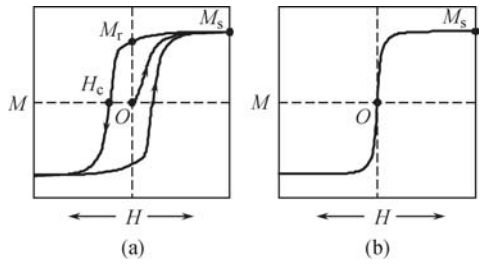


**Fig. 1** Schematic illustration of **(a)** a typical hysteresis loop of an array of single-domain FM NPs and **(b)** a typical curve for an array of SPM NPs.

In these NPs, the magnetization reversal process is dominated by coherent rotation of magnetic easy axis and the magnetization switching rate is determined by $\tau = \tau_0 e^{K_u V/(2kT)}$ ($\tau$ : relaxation time, $K_u$: anisotropic constant, $V$: particle volume, $k$: Boltzmann constant, and $T$: temperature). $K_u V$ represents the magnetic anisotropy energy (the energy barrier between the two orientations), while $kT$ stands for thermal energy [4, 5]. When these NPs are shrunk to a level that $kT$ is comparable to $K_u V$, they become magnetically unstable and in the absence of an external magnetic field, their magnetization is randomized and the overall magnetic moment is zero. These NPs are said to be superparamagnetic (SPM) [6]. Figure 1(b) shows the hysteresis loop of a group of SPM NPs. Because of thermal activation, these SPM NPs have no coercivity, i.e., they can be magnetized to achieve $M_s$, but their magnetization directions are randomized once the external magnetic field is switched off. This superparamagnetism of the small FM NPs can be blocked by lowering the temperature to a level below which they are FM [5]. The ferromagnetism to superparamagnetism transition has become a physical limit to the applications of FM NPs in magnetic data storage [7] or magnetic energy storage. However, the SPM NPs have been proven to be ideal for biomedical applications due to the lack of strong magnetic interactions between the dispersed NPs in the absence of an external magnetic field. The bio-related applications of these magnetic NPs have been summarized in other papers [8–12]. In this review, we mainly discuss the chemical synthesis and assembly of magnetic NPs for magnetic data storage and magnetic energy storage applications [8, 13, 14].

## 2 Chemical synthesis of magnetic NPs

Among all magnetic NPs studied, Fe, Co and their alloy NPs have attracted much attention due to the high magnetic moments in Fe, Co and FeCo (Co, 1422 emu/cc; Fe, 1714 emu/cc; $Fe_{65}Co_{35}$, 1950 emu/cc), and large anisotropy constants (equal to large coercivity) in FePt and SmCo (FePt, 7 MJ/m$^3$; $SmCo_5$, 14 MJ/m$^3$) for magnetic applications. Compared to various physical deposition methods, solution phase syntheses have shown great advantage in controlling NP size, shape, composition and nanomagnetic properties [10]. Here we focus on recent developments in solution-phase syntheses of monodisperse Fe, Co, CoFe, FePt and $SmCo_5$ NPs.

### 2.1 Syntheses of Fe and Co NPs

Metal carbonyls and their related derivatives are one representative class of organometallic complexes applied to the synthesis of metallic NPs. When heated, these metal carbonyls release CO, leaving zero-valent metal centers to nucleate and grow into NPs [10]. By thermal decomposition of iron(0) pentacarbonyl ($Fe(CO)_5$) in dioctyl ether and with oleic acid (OA) and oleylamine (OAm) as surfactants, Fe NPs with size ranging from 5 nm to 19 nm were synthesized [15, 16]. By decomposition of $\{Fe[N(SiMe_3)_2]_2\}_2$ in the presence of palmitic acid and hexadecylamine, 1.5 nm to 27 nm Fe NPs with various shapes (spheres, cubes, or stars) were made [17]. Compared to the Fe NPs made from the $Fe(CO)_5$ decomposition, those produced from the $\{Fe[N(SiMe_3)_2]_2\}_2$ precursor show better crystallinity. However, Fe NPs obtained from both methods are air-sensitive, making the characterization of metallic Fe NPs extremely challenging. Specifically, the $\{Fe[N(SiMe_3)_2]_2\}_2$ decomposition method requires reductive atmosphere of dihydrogen, and the reactants and products have to be stored and manipulated in an argon glove box. Figure 2(a) shows TEM images of 20.9 nm cubic Fe NPs prepared with this method.

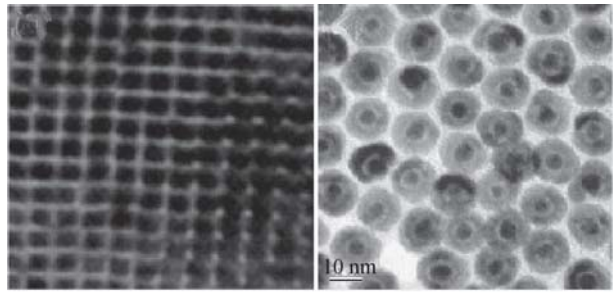


**Fig. 2** TEM images of **(a)** 20.9 nm cubic Fe NPs and **(b)** 5 nm/5 nm $Fe/Fe_3O_4$ NPs prepared by controlled oxidation of Fe NPs. Reproduced from Refs. [17, 18] with permission from the American Chemical Society.

$Fe_3O_4$ coating can be applied to protect Fe NPs from further oxidation [18]. In this approach, monodisperse Fe NPs were first prepared by thermal decomposition of $Fe(CO)_5$ in 1-octadecene (ODE) and OAm at 180°C. Before the reaction system was exposed to air, trimethylamine N-oxide, ($Me_3NO$), was introduced to control the Fe oxidation process at 250°C. This controlled oxidation gives core/shell structured $Fe/Fe_3O_4$ in which $Fe_3O_4$ has inverse spinel structure and acts as an anti-oxidation layer. Figure 2(b) shows the TEM image of $Fe/Fe_3O_4$ core/shell NPs. The thickness of the shell was tuned by controlling the amount of $Me_3NO$ added into the reaction mixture. After this treatment, the chemical and dispersion stabilities of the particles are improved dramatically. For $Fe/Fe_3O_4$ NPs containing 4 nm (radius) Fe core and 2.5 nm $Fe_3O_4$ shell, their saturation magnetization reaches 123.5 emu/g [Fe] ([Fe] = Fe+$Fe_3O_4$). Taking into account the lower magnetization caused by the presence of the $Fe_3O_4$, the saturation magnetization of the Fe core is close to the bulk value of 218 emu/g.

Fe NPs can also be synthesized from the reduction of Fe (III) and Fe (II) precursors. It is known that

reduction of iron (III) acetylacetonate ($Fe(acac)_3$) with 1,2-hexadecanediol in benzyl ether with OA and OAm as surfactants gave $Fe_3O_4$ NPs [19]. A further test showed that excess diol could reduce $Fe_3O_4$ into Fe, giving a mixture of metallic bcc-Fe and Fe oxide phases [20]. Furthermore, a high-temperature (380°C) reduction of Fe (II) stearate in the presence of sodium oleate has led to the formation of Fe nanospheres, nanocubes and nanoframes. The reducing agents in this case are C, CO, and/or $H_2$– species coming from the high temperature decomposition of OA [21, 22].

Metal carbonyl decomposition and metal salt reduction are also commonly used to make Co NPs. Depending on reaction conditions, Co NPs with controlled structures have been synthesized. For example, Co NPs with multiple twinned face centered cubic (fcc) structure were made by decomposing $Co_2(CO)_8$ in diphenylether (DPE) with OA and tributylphosphines (TBP) as surfactants [23]. Co NPs with $\varepsilon$-Co structure were synthesized by either decomposing $Co_2(CO)_8$ in o-dichlorobenzene with OA, lauric acid and trioctylphosphine oxide (TOPO) as surfactants [24], or by superhydride ($LiBEt_3H$) reduction of $CoCl_2$ in dioctylether with OA and trialkylphosphine as surfactants. The mechanism leading to the formation of Co NPs with different structures is still not clear. The syntheses do indicate that NP growth seems to be sensitive to the chemical nature of alkylphosphine and its molar ratio with OA and Co precursor. Interestingly, $\varepsilon$-Co was found to be metastable and could be converted to hexagonal close packed (hcp) Co NPs by annealing at 300°C and further to fcc-Co NPs at 450°C [25]. Nearly monodisperse cobalt nanorods were synthesized by thermal decomposition of $[Co(\eta^3\text{-}C_8H_{13})(\eta^4\text{-}C_8H_{12})]$ in the presence of a mixture of hexadecylamine (HDA) and aliphatic acid [26]. The aspect ratios of these Co nanorods were controlled by the length of the hydrocarbon chain in aliphatic acid with short-chain aliphatic acid leading to the shorter and wider rods.

Recently, monodisperse hcp Co NPs were synthesized directly by reducing $Co(CH_3COO)_2{\cdot}4H_2O$ with 1,2-dodecanediol in the presence of DPE, OA and TOP [23]. Hollow fcc Co NPs were made by reducing fcc CoO NPs in OAm at 290°C. In this hollow Co NP synthesis, the size and shape of the NPs remained the same throughout the chemical transformation from CoO to Co [27]. The long-term stability of the Co NPs can be improved drastically by coating them with $MFe_2O_4$ (M = Fe, Mn) ferrite shell [28].

### 2.2 Syntheses of FeCo, FePt and $SmCo_5$ NPs

The alloy NPs of FeCo, FePt and $SmCo_5$ represent three important classes of FM NPs with FeCo having the highest magnetic moment among all FM materials, and FePt and $SmCo_5$ showing the largest anisotropy constant ($K_u$) and coercivity. FePt can be made chemically stable and is an excellent model system for studying nanoscale magnetism [29]. The rare-earth metal based hard magnetic $SmCo_5$ NPs are promising for high temperature magnetic applications but preparation and stabilization of $SmCo_5$ NPs have been extremely challenging thus far.

High moment FeCo NPs were made by simultaneous thermal decomposition of $Fe(CO)_5$ and $Co_2(CO)_8$ in 1,2-dichlorobenzene with OA as surfactant [30], or reductive thermal decomposition of $Fe(CO)_5$ and $Co(\eta^3\text{-}C_8H_{13})(\eta^4\text{-}C_8H_{12})$ or $Co(N(SiMe_3)_2)_2$ in the presence of 1 equiv of hexadecylamine and 1 equiv of oleic acid [31]. FeCo NPs were also synthesized by reduction of $Fe(acac)_3$ and $Co(acac)_3$ with 1,2-hexadecanediol in OA and OAm under an Ar + 7% $H_2$ atmosphere [32]. The 20 nm NPs have a magnetization value of 207 emu/g. Recently, high moment CoFe NPs were prepared by coating Co NPs with a layer of Fe followed by inter-diffusion of Co and Fe [33]. The stability of the CoFe NPs can be enhanced by embedding them into a carbon matrix [34]. In the synthesis, Fe and Co salts were first absorbed onto the high surface-area silica powder by impregnation in a methanol solution. The metal-loaded silica was dried at 800°C under $H_2$ and then subjected to methane chemical vapor deposition (CVD) for carbon deposition on FeCo. Once cooled down to room temperature, the silica was etched away in HF, leaving pure FeCo/graphitic carbon NPs that showed dramatic stability against deep oxidation.

Although monodisperse FePt NPs can be synthesized by superhydride reduction of $FeCl_2$ and $Pt(acac)_2$ in diphenylether, OA, OAm and 1,2-hexadecanediol [35], a more popular method for making FePt NPs is via a combination of thermal decomposition of metal carbonyl and metal salt reduction. For example, simultaneous thermolysis of $Fe(CO)_5$ and reduction of $Pt(acac)_2$ in the presence of 1,2-hexadecanediol led to the formation of monodisperse FePt NPs [36, 37]. Cubic FePt NPs were synthesized in the absence of 1,2-hexadecanediol, as shown in the TEM image in Fig. 3(a), and the cubic shape was realized by controlling the addition sequence of OA and OAm [38]. More recently, FePt nanowires (NWs) and nanorods (NRs) from 200 to 20 nm long were synthesized by reduction of $Pt(acac)_2$ and thermal decomposition of $Fe(CO)_5$ in a mixture of OAm and ODE. The length of the FePt NWs/NRs was tuned by the volume ratio of OAm/ODE [39]. Figure 3(b) shows a TEM image of the 50 nm $Fe_{55}Pt_{45}$ NWs. All FePt NPs mentioned above have the face centered cubic (fcc) structure and are superparamagnetic at room temperature. Thermal annealing (>500°C) is required to convert fcc to face centered tetragonal (fct) structure that is ferromagnetic at room temperature. However, this high temperature annealing often causes serious NP aggregation/sintering, deteriorating the NP quality. To avoid this aggregation/

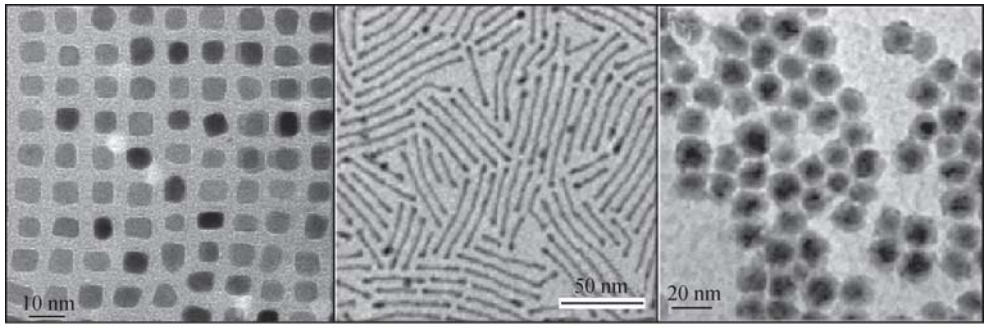


**Fig. 3** TEM images of **(a)** 6.9 nm $Fe_{50}Pt_{50}$ nanocubes; **(b)** 50 nm $Fe_{55}Pt_{45}$ nanowires; and **(c)** $Co/Sm_2O_3$ nanoparticles. Reproduced from Refs. [38, 39, 46] with permission from the American Chemical Society and the Wiley-VCH Verlag GmbH & Co.

sintering problem, FePt NPs were either coated with $SiO_2$ [40, 41], or MgO [42, 43], or ground with a large excess of NaCl [44, 45] before high temperature annealing was applied. Using these protecting methods and high temperature annealing, various hard magnetic fct-FePt NPs with coercivity as large as 40 kOe have been synthesized.

Different from the synthesis of FeCo and FePt NPs, preparation of SmCo alloy NPs is even more challenging due to the extreme chemical reactivity of rare-earth metal Sm in nanoscale. Early attempts in using 1,2-hexadecanediol reduction of $Sm(acac)_3$ and thermolysis of $Co_2(CO)_8$ in dioctyl ether with OA and OAm as surfactants led to 6–8 nm $SmCo_5$ NPs. However, magnetic data indicated that these NPs did not have the hard magnetic phase as they had a coercivity of only 2.2 kOe at 5 K and was superparamagnetic at room temperature [47]. Recently, $SmCo_5$ nanocrystalline hard magnets were prepared by reductive annealing of core/shell structured $Co/Sm_2O_3$ NPs [Fig. 3(c)] at 900°C in the presence of KCl and metallic Ca. Here KCl was used as the dispersion medium at the reduction temperature to prevent NPs from growing into large single crystals and metallic Ca was used as a reducing agent. The coercivity of these $SmCo_5$ nanocrystalline magnets reached 24 kOe at 100 K and 8 kOe at room temperature [46].

## 3 Magnetic NP assembly

The assembly of magnetic NPs in a well-defined manner is crucial for their potential in high-density data storage and high-density energy storage applications [8]. There are variable approaches to construct NP assemblies in highly ordered long-range periodic structures, namely "NP superlattices". In this section, we briefly discuss NP self-assembly and polymer-mediated NP assembly.

The monodisperse NPs suspended in solution tend to form ordered arrays after solvent evaporation. This assembly tendency is influenced by the nature of the interactions exhibited among the stabilized NPs. The synthetic strategy to NP superlattices relies on a large number of weak and non-directional interactions, such as ionic bonds, hydrogen bonds and van der Waals interactions to organize the particles-self-assembly. It is the most common way to obtain long-range-ordered NP superlattices [48, 49]. Figure 4(a) illustrates the formation of a well-organized NP superlattice by slow evaporation of the solvent from the NP dispersion that spreads on a solid substrate. Similarly, the formation of self-assembled magnetic NPs is through the van der Waals, hydrogen bonding, magnetic interaction, and the repulsion that can be controlled by NP concentration, NP morphologies, NP coating, solvent volatility and chemical nature of the substrate [50]. Various 2-D and 3-D superlattices of magnetic NPs including spherical NPs

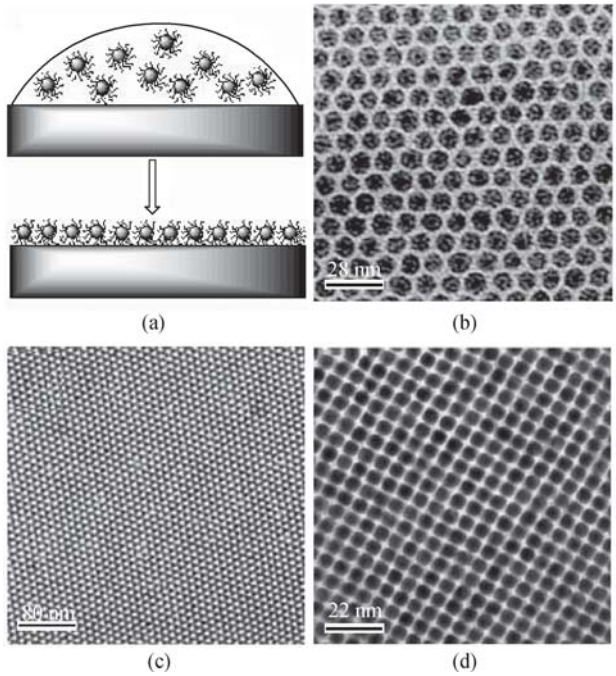


**Fig. 4** **(a)** Schematic illustration of NP self-assembly via solvent evaporation, and **(b)** TEM image of a 2-D assembly of 10 nm cobalt nanoparticles [Both Fig. 4(b) and (c) from our lab], **(c)** TEM image of a 3-D assembly of 8 nm cobalt nanoparticles (from our lab), and **(d)** TEM image of a 3-D assembly of 6 nm $Fe_{50}Pt_{50}$ nanoparticles. Reproduced from Ref. [37] with permission from American Association for the Advancement of Science.

[18, 25], cubic NPs [38, 51], nanorods [52], nanowires [39], and hollow NPs [53] have been obtained. Figure 4(b)–(d) are representative TEM images of a 2-D assembly of 10 nm cobalt NPs, a 3-D assembly of 8 nm cobalt NPs and a 3-D assembly of 6 nm $Fe_{50}Pt_{50}$ NPs. NP concentration in the dispersion is one of the most convenient parameters used to tune the assembly in 2-D or 3-D structure. In these self-assembled NP superlattices, interparticle spacings were normally tuned by the length of the surfactants surrounding each NP [37].

NP superlattices can also be formed by slowly drying NP dispersion on a water surface through the Langmuir–Blodgett (LB) technique [54, 55]. 10–30 μm FePt colloidal crystals were made by a three layer solvent diffusion technique [56]. In this approach, a buffer layer was sandwiched in two solvent layers and facilitated the slow diffusion of a non-solvent into the NP dispersion for the growth of the 3-D NP superlattice.

Although self-assembly can lead to NP superlattices with controlled NP distance and assembly structure, it is difficult to control the lateral dimension and thickness of the assemblies. To achieve large area assembly with desired NP packing thickness and density, various polymers with specific functional groups are often used to mediate the NP assembly. The functional polymer can be chosen to adhere to a solid substrate, and NPs attach to the polymer via their binding to the functional group(s) on the polymer. The NPs without direct binding to the polymer can be washed away, leaving a monolayer NP assembly on the substrate [57, 58]. Multiple layers of NPs can be constructed similarly by repeating the same procedure for several times [59–61]. Several polymers have been demonstrated to have capacity in assembling magnetic NPs. Polyethylenimine (PEI)-FePt assemblies were fabricated by dipping the substrate into PEI solution and FePt NP dispersion solution alternately followed by fresh solvent wash [35, 62]. The PEI-FePt assemblies exhibited controlled thickness and smooth surface as analyzed by X-ray reflectivity and AFM. Similarly, phospholipid-FePt [63], oleic acid/oleylamine-FePt [64], and amino-functional silane ([3-(2-aminoethlyamino) propyl] trimethoxysilane, APTS)-FePt [65] were also prepared. The APTS-FePt nanocomposite film showed no significant coalescence of the FePt NPs after annealing at 800°C that transformed the as-synthesized SPM fcc-FePt NPs to magnetically hard fct-FePt NPs.

Block-copolymer (BCP) has been used to encapsulate the as-synthesized hydrophobic NPs by forming an NP-micelle bilayer structure [66, 67]. In this assembly process, a concentrated NP dispersion in organic solvent was added to an aqueous solution of BCP under vigorous stirring to form an oil-in-water micro-emulsion. During the evaporation of the organic solvent, the hydrophobic blocks of BCP interdigitate into the alkane chain on the NP surface driven by hydrophobic interactions and create a thermodynamically stable NP-micelle bilayer structure [66, 68]. Both 2D and 3D NP superlattices have been fabricated using these NP-micelles as building blocks with NP packing density controlled by the size of the polymer component in BCP [67–73].

## 4 Magnetic NP assemblies for information storage applications

Hard-disk-based magnetic recording is currently the dominant data storage technique in various information applications. The components of a hard disk drive are the recording head and the magnetic storage media. The recording head contains separate read and write elements that allow the disk to be written and read longitudinally with the magnetization of the recorded bit lying in the plane of the disk [Fig. 5(a)] [7, 74, 75]. The recorded bits have two stable magnetization states, corresponding to $M_r$ and $-M_r$ in the magnetic hysteresis loop. Conventional recording media are fabricated in the form of granular thin film consisting of weakly coupled magnetic particles of CoPtCrX alloy (X = B, Ta) with sizes of 8–10 nm [Fig. 5(b)] [75]. Each recording bit corresponds to the averaged remnant magnetization of hundreds of isolated FM CoPtCrX grains.

Today, the increasing demands for information storage require much faster progression of the recording density of a hard disk drive. The most direct way to increase the storage density is to develop smaller magnetically stable grains (NPs) with weak magnetic interaction between neighboring grains [7]. Narrowing grain size distribution as well as reducing grain size can maintain the signal-to-noise ratio (SNR) of the media at an acceptable level. However, further decrease of the current grain size of CoPtCrX alloy may cause the magnetic anisotropy energy (energy barrier) comparable to the thermal energy and the demagnetization (SPM behavior) of the storage media at room temperature. The magnetic anisotropy energy to thermal energy $[K_uV/(k_BT)]$ ratio of 50–70 is believed to be the minimum for a thermally stable medium that preserves the recorded information for at least 10 years [75]. Since the energy barrier is proportional to $K_uV$, high $K_u$ material, such as $L1_0$ ordered FePt and CoPt alloys are clearly the promising candidates for smaller magnetically stable grains [76, 77]. Other recording techniques, such as perpendicular magnetic recording (PMR) [78] and thermally assisted magnetic recording (TAMR) [79, 80] enable the use of data storage medium with very high anisotropy constant that cannot be written by conventional longitudinal magnetic recording (LMR) technique. In addition, PMR can further improve the areal storage density since it permits smaller bit size due to the possible reduction of

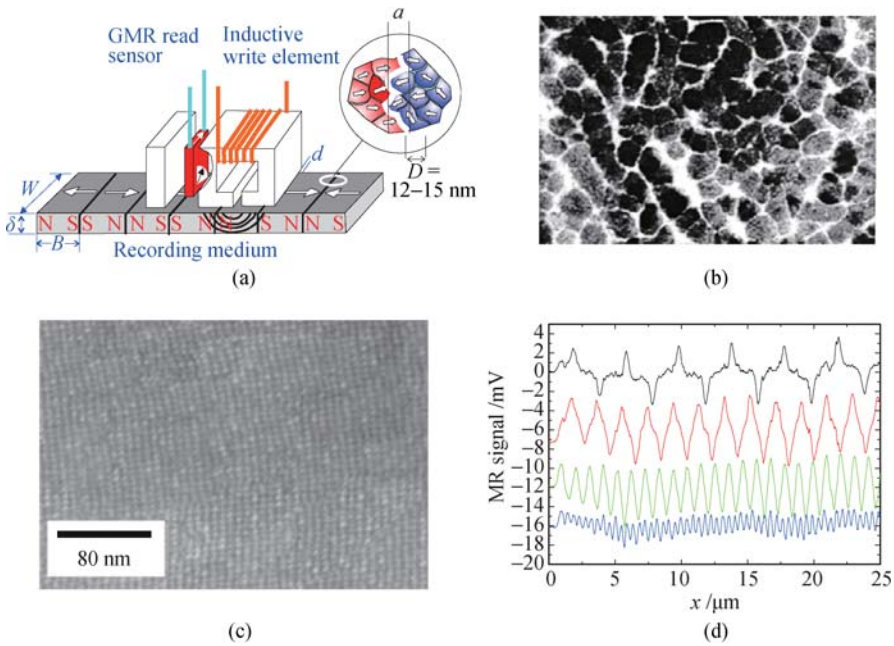


**Fig. 5** **(a)** Schematic illustration of a longitudinal recording system. Shown in the figure is the recording head and medium with one bit dimension in $B \times W \times \delta$ and transition gap between two bits in $a$. **(b)** A TEM image of modern CoCrPtB recording media with an average grain diameter of 9 nm. **(c)** An HRSEM image of a ∼180-nm-thick, 4 nm $Fe_{52}Pt_{48}$ nanocrystal assembly annealed at 560°C for 30 min under 1 atm of $N_2$ gas. **(d)** Magneto-resistive (MR) read-back signals from written bit transitions in a 120 nm thick assembly of 4 nm $Fe_{48}Pt_{52}$ nanocrystals. The individual line scans reveal magnetization reversal transitions at linear densities (from top to bottom) of 500, 1040, 2140, and 5000 fc/mm. Reproduced from Refs. [74, 37] with permission from the American Institute of Physics Publishing and American Association for the Advancement of Science.

transition width [$a$ in Fig. 5(a)] in the bit cell. Overall, well-organized 2-D assemblies of monodisperse FM NPs ($\sigma < 5\%$) with high anisotropy constant and coated with a thin non-magnetic layer are promising for high density data storage applications [7].

The fct-structured FePt has an anisotropy constant as high as (4–10) × $10^7$ erg·cm$^{-3}$ [76, 77], which is at least 50 times higher than that of currently used CoPtCrX alloy. The extremely high $K_u$ of FePt allows them to be magnetically stable at a grain size as small as 3 nm, which means a potential 10-fold areal density increase as recording media [7]. Previous work has demonstrated that self-assembled FM FePt NP arrays are promising candidates for high-density data storage media [37]. By thermal annealing at 540°C for 30 min, a smooth FM $Fe_{48}Pt_{52}$ NP array with room temperature coercivity of 1800 Oe was obtained from a SPM $Fe_{48}Pt_{52}$ NP array. The high-resolution scanning electron microscopy (HRSEM) image of a ∼120-nm-thick 4 nm FM NP assembly used for the writing experiment is shown in Fig. 5(c). Using a static write/read tester, the read-back sensor voltage signals from the written data tracks were recorded, with linear densities of 500, 1040, 2140, and 5000 flux changes per millimeter [Fig. 5(d)]. This preliminary recording experiment indicated that the FM FePt NP assembly can indeed support magnetization reversal transitions at moderate linear densities that can be read back nondestructively.

Recording experiments on FM FePt NP array with larger coercivity were also demonstrated by thermally assisted recording technique [62]. A three-layer 4 nm $Fe_{58}Pt_{42}$ assembly annealed at 530°C under Ar + $H_2$ (5%) for 30 min had a coercivity of 5 kOe at room temperature that would not allow the writing using conventional recording technique since the magnetization of the assembly cannot be saturated or reversed. The annealed assembly was treated with a sharply focused laser diode beam (beam diameter 1 μm, wavelength 660 nm) with fast pulses (<100 ns) under a perpendicular magnetic field of 2.5 kOe. The temperature of the assembly after laser treatment can reach over 200°C and the coercivity of the array was reduced, which allowed the particles to be addressed by a weak magnetic bias field. The atomic force microscopy (AFM) image and magnetic force microscopy (MFM) image showed that the array was intact after the laser treatment and the NP magnetization pointing to the out-of-NP-assembly plane.

## 5 Magnetic NP assemblies for energy storage applications

Permanent magnets have been widely used as energy storage materials in devices such as motors and generators. Maximum energy product $(BH)_{max}$ is used to evaluate the energy-storage ability of a permanent

magnet. It is defined by the area of the largest rectangle that can fit inside the second quadrant of a $B$–$H$ loop derived from the $M$–$H$ loop *via* the relation of $B = u_0M + H$ [Fig. 6(a)]. Generally, both high remnant magnetization ($M_r$) and high coercivity ($H_c$) are crucial for permanent magnets to have high $(BH)_{max}$. However, high magnetic moment and large coercivity are incompatible in single-phase magnets. Magnetically soft materials (Fe, Co, or FeCo) have very high magnetic moment, but their coercivities are low (<1 kOe), which makes them unsuitable as energy storage materials. The energy storage materials currently used are hard magnets that have very large coercivity but relatively low moment compared with the soft magnetic materials.

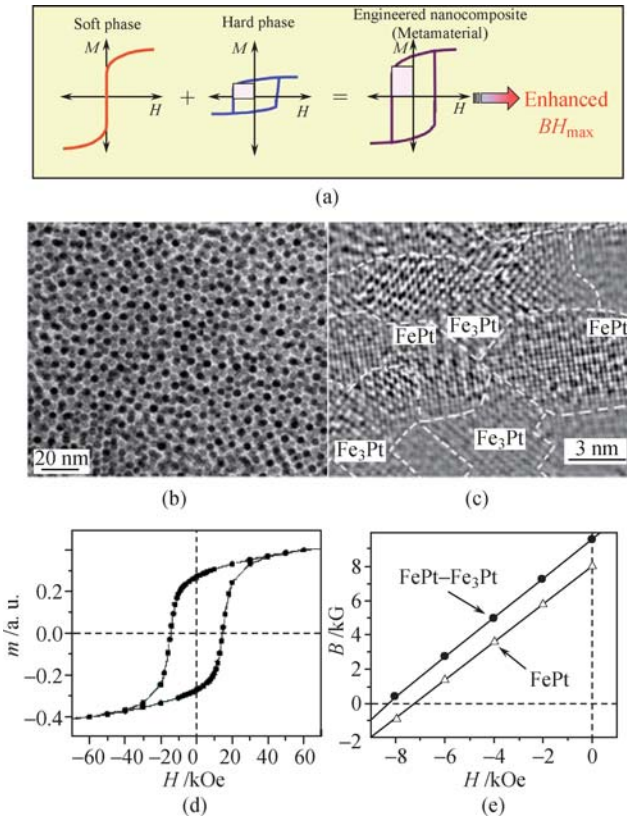


**Fig. 6** **(a)** Schematic illustration of hysteresis behavior of a nanocomposite magnet consisting of both magnetically soft and magnetically hard phases that interact by magnetic exchange-coupling across the interface. **(b)** TEM image of the binary assembly of 4 nm FePt NPs and 4 nm $Fe_3O_4$ NPs. **(c)** HRTEM image of the FePt–$Fe_3Pt$ nanocomposite. **(d)** Magnetic hysteresis loop of the composite shown in (c). **(e)** Second-quadrant $B$–$H$ curves of the hysteresis loops of the FePt–$Fe_3Pt$ composite and the annealed 4 nm FePt array. Reproduced from Ref. [14] with permission from Nature Publishing Group.

Current advances in materials fabrication have made single-phase magnets with the $(BH)_{max}$ approaching their theoretical limit. For example, $Nd_2Fe_{12}B$ magnets were made with $(BH)_{max}$ = 474 kJ/m$^3$ [81], 90% of the theoretical limit at 512 kJ/m$^3$–the highest for a single-phase magnet [82]. However, due to the low Curie temperature of the $Nd_2Fe_{12}B$ alloy (310°C), the $Nd_2Fe_{12}B$ magnets can only be operated at normal temperature. With Curie temperature at 727°C, $SmCo_5$ alloy is clearly a better magnet candidate for high temperature applications. However, its low magnetization results in low energy product with the theoretical value at 219 MJ/m$^3$ [83]. Therefore, further efforts should be focused on SmCo alloys with energy product surpassing the limit of single-phase magnets.

Nanocomposite magnets consisting of both magnetically soft and hard phases that interact by magnetic exchange-coupling across the interface are promising systems to achieve maximum energy products far beyond the limit of single-phase magnets [84]. An exchange-coupled magnetic nanocomposite retains both the high magnetization from the soft phase and the large coercivity from the hard phase, and exhibits a smooth, single-phase-like hysteresis behavior. Recent model tests have shown that $(BH)_{max}$ up to 1 MJ/m$^3$ can be achieved by optimally coupled composites with a multilayer structure in less than 10 nm and composed of alternating hard and soft magnetic periodicities [85].

Exchange-spring nanocomposites with controlled soft phase size were first demonstrated in the FePt–$Fe_3Pt$ system [14]. It was fabricated by self-assembly of FePt and $Fe_3O_4$ NPs and reductive annealing at 650°C for 1 hour. During the annealing of the 4 nm-4 nm FePt–$Fe_3O_4$ assembly with 1:10 mass ratio [Fig. 6(b)], the fcc-FePt was transformed into fct-FePt and the $Fe_3O_4$ was reduced to metallic Fe that further underwent inter-diffusion with FePt to give $Fe_3Pt$. The exchange-spring nanocomposite had a soft phase of $Fe_3Pt$ (∼5 nm) embedded in FePt matrix [Fig. 6(c)], a smooth hysteresis loop [Fig. 6(d)], and an energy product of 160 kJ/m$^3$ that exceeds 117 kJ/m$^3$ from the single-phased $Fe_{58}Pt_{42}$ assembly by 37% [Fig. 6(e)] [86]. The FePt-based nanocomposite can also be made by self-assembly of core/shell structured FePt/$Fe_3O_4$ NPs followed by reductive annealing [87]. The nanocomposite made from 4 nm/1 nm FePt/$Fe_3O_4$ NPs had an energy product of 144 kJ/m$^3$.

SmCo-based permanent magnets are superior for high-temperature applications due to their large anisotropy constant (up to 2.0 × 10$^8$ erg·cm$^{-3}$), and high Curie temperature ($T_c$ = 1020 K) [46]. In a recent demonstration, SmCo/Fe exchange-coupled nanocomposites were fabricated by embedding $Fe_3O_4$ NPs in the matrix of Sm–Co oxides followed by a high-temperature reductive annealing [88]. During the process, $Fe_3O_4$ NPs were first synthesized, transferred into water phase by ligand replacement, and co-precipitated with $SmCl_3$ and $CoCl_2$ by adding ammonium base in an aqueous solution. The mixture was then baked at 120°C to remove water. The composite oxide powder was further mixed with Ca and KCl and annealed at 900°C for 1 hour. The SmCo/$Fe_{1.5}$ nanocomposite made from this process had a remnant magnetic moment of 56 emu/g. This magnetic moment value is 25% higher than that of the pure $SmCo_5$ alloy

magnet obtained by the same reduction method. Further optimization of these nanocomposites with controlled size and composition on both soft and hard phases are still needed to achieve a high energy product.

## 6 Conclusion and future outlook

In this review, we have summarized recent advances in chemical syntheses of monodisperse magnetic NPs of Fe, Co as well as their alloy NPs of FeCo, FePt and $SmCo_5$. Fe, Co and FeCo NPs have been made with magnetic moment reaching the bulk value and their air-stability are better controlled by iron oxide coating. SPM FePt NPs synthesized from the organic solution phase are readily converted into FM FePt NPs via high temperature annealing. The problems in FePt NP aggregation/sintering under this high temperature annealing conditions are solved by coating the FePt NPs with inorganic materials of $SiO_2$, MgO or NaCl. These FM NPs and their assemblies show great potential for high-density information storage media and energy storage applications.

However, there are still tremendous challenges ahead in using these NPs as building blocks to fabricate practical magnetic devices. In self-assembled FePt NP array, the long-range NP ordering in both texture and magnetic easy axis has not been established. The NPs are also difficult to pack in ultrahigh density with interparticle spacing less than 1 nm. Because of the lack of these controls in NP assembly, magnetic switching behaviors from each single NP in an NP array have not been studied. Furthermore, despite their potential for ultrahigh density magnetic recording applications, FePt NPs are not suitable for the fabrication of bulk magnets due to the limiting factors from Pt. The nanocomposite magnets for high temperature applications should be made from SmCo alloy NPs, but previous synthetic efforts have not yielded monodisperse SmCo NPs with promising FM properties. Therefore, syntheses of FM NPs, especially SmCo alloy NPs, and controls of magnetic easy axis alignment in FM NP arrays are two important directions in chemical synthesis and self-assembly of magnetic NPs for high density magnetic information storage and magnetic energy storage applications.

**Acknowledgements** The work at Brown University was supported by ONR/MURI N00014-05-1-0497 and DARPA/ARO W911NF-08-1-0249.

## References

1. B. D. Cullity, Introduction to Magnetic Materials, Reading, MA: Addison Wesley Publishing Company, 1972
2. A. Aharoni, Introduction to the Theory of Ferromagnetism, New York: Oxford University Press, 1996
3. R. Skomski and J. M. D. Coey, Permanent Magnetism, Bristol, UK and Philadelphia, PA: Institute of Physics Publishing, 1999
4. E. C. Stoner and E. P. Wohlfarth, Philos. Trans. R. Soc. London A, 1948, 240(826): 599
5. L. Néel, C. R. Acad. Sci., 1949, 228: 664
6. C. P. Bean, J. Appl. Phys., 1955, 26: 1381
7. D. Weller and M. F. Doerner, Annu. Rev. Mater. Sci., 2000, 30: 611
8. S. H. Sun, Adv. Mater., 2006, 18(4): 393
9. C. J. Xu and S. H. Sun, Polymer International, 2007, 56(7): 821
10. N. A. Frey, S. Peng, K. Cheng, and S. H. Sun, Chem. Soc. Rev., 2009, 38(9): 2532
11. C. Sun, J. S. H. Lee, and M. Q. Zhang, Adv. Drug Deliv. Rev., 2008, 60(11): 1252
12. L. M. Lacroix, D. Ho, and S. H. Sun, Curr. Top. Med. Chem., 2010, 10(12): 1184
13. J. P. Wang, Proc. IEEE, 2008, 96(11): 1847
14. H. Zeng, J. Li, J. P. Liu, Z. L. Wang, and S. H. Sun, Nature, 2002, 420(6914): 395
15. D. Farrell, S. A. Majetich, and J. P. Wilcoxon, J. Phys. Chem. B, 2003, 107(40): 11022
16. D. L. Huber, Small, 2005, 1(5): 482
17. L. M. Lacroix, S. Lachaize, A. Falqui, M. Respaud, and B. Chaudret, J. Am. Chem. Soc., 2009, 131(2): 549
18. S. Peng, C. Wang, J. Xie, and S. H. Sun, J. Am. Chem. Soc., 2006, 128(33): 10676
19. S. H. Sun, H. Zeng, D. B. Robinson, S. Raoux, P. M. Rice, S. X. Wang, and G. X. Li, J. Am. Chem. Soc., 2004, 126(1): 273
20. S. Yamamuro, T. Ando, K. Sumiyama, T. Uchida, and I. Kojima, Jpn. J. Appl. Phys. Part 1: Regul. Pap. Short Notes Rev. Pap., 2004, 43(7A): 4458
21. D. Kim, J. Park, K. An, N. K. Yang, J. G. Park, and T. Hyeon, J. Am. Chem. Soc., 2007, 129(18): 5812
22. J. Park, K. J. An, Y. S. Hwang, J. G. Park, H. J. Noh, J. Y. Kim, J. H. Park, N. M. Hwang, and T. Hyeon, Nature Materials, 2004, 3(12): 891
23. C. B. Murray, S. H. Sun, H. Doyle, and T. Betley, MRS Bulletin, 2001, 26(12): 985
24. V. F. Puntes, K. M. Krishnan, and P. Alivisatos, Appl. Phys. Lett., 2001, 78(15): 2187
25. S. H. Sun and C. B. Murray, J. Appl. Phys., 1999, 85(8): 4325
26. F. Dumestre, B. Chaudret, C. Amiens, M. Respaud, P. Fejes, P. Renaud, and P. Zurcher, Angewandte Chemie-International Edition, 2003, 42(42): 5213
27. K. M. Nam, J. H. Shim, H. Ki, S. I. Choi, G. Lee, J. K. Jang, Y. Jo, M. H. Jung, H. Song, and J. T. Park, Angewandte Chemie-International Edition, 2008, 47(49): 9504
28. S. Peng, J. Xie, and S. H. Sun, J. Solid State Chem., 2008, 181(7): 1560
29. C. Antoniak, J. Lindner, M. Spasova, D. Sudfeld, M. Acet, M. Farle, K. Fauth, U. Wiedwald, H. G. Boyen, P. Ziemann, F. Wilhelm, A. Rogalev, and S. H. Sun, Phys. Rev. Lett., 2006, 97(11): 117201

30. A. Hutten, D. Sudfeld, I. Ennen, G. Reiss, K. Wojczykowski, and P. Jutzi, J. Magn. Magn. Mater., 2005, 293(1): 93
31. C. Desvaux, C. Amiens, P. Fejes, P. Renaud, M. Respaud, P. Lecante, E. Snoeck, and B. Chaudret, Nature Materials, 2005, 4(10): 750
32. G. S. Chaubey, C. Barcena, N. Poudyal, C. B. Rong, J. M. Gao, S. H. Sun, and J. P. Liu, J. Am. Chem. Soc., 2007, 129(23): 7214
33. C. Wang, S. Peng, L. M. Lacroix, and S. H. Sun, Nano Research, 2009, 2(5): 380
34. W. S. Seo, J. H. Lee, X. M. Sun, Y. Suzuki, D. Mann, Z. Liu, M. Terashima, P. C. Yang, M. V. Mcconnell, D. G. Nishimura, and H. J. Dai, Nature Materials, 2006, 5(12): 971
35. S. H. Sun, S. Anders, T. Thomson, J. E. E. Baglin, M. F. Toney, H. F. Hamann, C. B. Murray, and B. D. Terris, J. Phys. Chem. B, 2003, 107(23): 5419
36. S. H. Sun, E. E. Fullerton, D. Weller, and C. B. Murray, IEEE Transactions on Magnetics, 2001, 37(4): 1239
37. S. H. Sun, C. B. Murray, D. Weller, L. Folks, and A. Moser, Science, 2000, 287(5460): 1989
38. M. Chen, J. Kim, J. P. Liu, H. Y. Fan, and S. H. Sun, J. Am. Chem. Soc., 2006, 128(22): 7132
39. C. Wang, Y. L. Hou, J. M. Kim, and S. H. Sun, Angewandte Chemie-International Edition, 2007, 46(33): 6333
40. S. Yamamoto, Y. Morimoto, T. Ono, and M. Takano, Appl. Phys. Lett., 2005, 87(3): 032503
41. Y. Tamada, S. Yamamoto, M. Takano, S. Nasu, and T. Ono, Appl. Phys. Lett., 2007, 90(16): 162509
42. J. Kim, C. B. Rong, Y. Lee, J. P. Liu, and S. H. Sun, Chem. Mater., 2008, 20(23): 7242
43. J. M. Kim, C. B. Rong, J. P. Liu, and S. H. Sun, Adv. Mater., 2009, 21(8): 906
44. D. R. Li, N. Poudyal, V. Nandwana, Z. Q. Jin, K. Elkins, and J. P. Liu, J. Appl. Phys., 2006, 99(8): 08E911
45. C. B. Rong, N. Poudyal, G. S. Chaubey, V. Nandwana, Y. Liu, Y. Q. Wu, M. J. Kramer, M. E. Kozlov, R. H. Baughman, and J. P. Liu, J. Appl. Phys., 2008, 103(7): 07E131
46. Y. L. Hou, Z. C. Xu, S. Peng, C. B. Rong, J. P. Liu, and S. H. Sun, Adv. Mater., 2007, 19(20): 3349
47. H. W. Gu, B. Xu, J. C. Rao, R. K. Zheng, X. X. Zhang, K. K. Fung, and C. Y. C. Wong, J. Appl. Phys., 2003, 93(10): 7589
48. C. B. Murray, C. R. Kagan, and M. G. Bawendi, Annu. Rev. Mater. Sci., 2000, 30: 545
49. C. B. Murray, S. H. Sun, W. Gaschler, H. Doyle, T. A. Betley, and C. R. Kagan, IBM Journal of Research and Development, 2001, 45(1): 47
50. D. H. Everett, Basic Principles of Colloid Science, Cambridge: Royal Society of Chemistry, 1988
51. H. Zeng, P. M. Rice, S. X. Wang, and S. H. Sun, J. Am. Chem. Soc., 2004, 126(37): 11458
52. M. Chen, T. Pica, Y. B. Jiang, P. Li, K. Yano, J. P. Liu, A. K. Datye, and H. Y. Fan, J. Am. Chem. Soc., 2007, 129(20): 6348
53. S. Peng and S. H. Sun, Angewandte Chemie-International Edition, 2007, 46(22): 4155
54. Q. J. Guo, X. W. Teng, and H. Yang, Adv. Mater., 2004, 16(15): 1337
55. T. Harada and T. A. Hatton, Langmuir, 2009, 25(11): 6407
56. E. Shevchenko, D. Talapin, A. Kornowski, F. Wiekhorst, J. Kotzler, M. Haase, A. Rogach, and H. Weller, Adv. Mater., 2002, 14(4): 287
57. G. Decher, Science, 1997, 277(5330): 1232
58. J. Schmitt, P. Machtle, D. Eck, H. Mohwald, and C. A. Helm, Langmuir, 1999, 15(9): 3256
59. Y. J. Liu, A. B. Wang, and R. Claus, J. Phys. Chem. B, 1997, 101(8): 1385
60. T. Cassagneau, T. E. Mallouk, and J. H. Fendler, J. Am. Chem. Soc., 1998, 120(31): 7848
61. J. F. Hicks, Y. Seok-Shon, and R. W. Murray, Langmuir, 2002, 18(6): 2288
62. S. H. Sun, S. Anders, H. F. Hamann, J. U. Thiele, J. E. E. Baglin, T. Thomson, E. E. Fullerton, C. B. Murray, and B. D. Terris, J. Am. Chem. Soc., 2002, 124(12): 2884
63. A. Terheiden, B. Rellinghaus, S. Stappert, M. Acet, and C. Mayer, J. Chem. Phys., 2004, 121(1): 510
64. M. Acet, C. Mayer, O. Muth, A. Terheiden, and G. Dyker, Journal of Crystal Growth, 2005, 285(3): 365
65. A. C. C. Yu, M. Mizuno, Y. Sasaki, M. Inoue, H. Kondo, I. Ohta, D. Djayaprawira, and M. Takahashi, Appl. Phys. Lett., 2003, 82(24): 4352
66. H. Y. Fan, K. Yang, D. M. Boye, T. Sigmon, K. J. Malloy, H. F. Xu, G. P. Lopez, and C. J. Brinker, Science, 2004, 304(5670): 567
67. H. Y. Fan, Chem. Commun., 2008, 12: 1383
68. H. Y. Fan, E. Leve, J. Gabaldon, A. Wright, R. E. Haddad, and C. J. Brinker, Adv. Mater., 2005, 17(21): 2587
69. H. Y. Fan, A. Wright, J. Gabaldon, A. Rodriguez, C. J. Brinker, and Y. B. Jiang, Adv. Funct. Mater., 2006, 16(7): 891
70. L. E. Euliss, S. G. Grancharov, S. O'brien, T. J. Deming, G. D. Stucky, C. B. Murray, and G. A. Held, Nano Lett., 2003, 3(11): 1489
71. H. Ai, C. Flask, B. Weinberg, X. Shuai, M. D. Pagel, D. Farrell, J. Duerk, and J. M. Gao, Adv. Mater., 2005, 17(16): 1949
72. B. Dubertret, P. Skourides, D. J. Norris, V. Noireaux, A. H. Brivanlou, and A. Libchaber, Science, 2002, 298(5599): 1759
73. B. S. Kim, J. M. Qiu, J. P. Wang, and T. A. Taton, Nano Lett., 2005, 5(10): 1987
74. A. Moser, K. Takano, D. T. Margulies, M. Albrecht, Y. Sonobe, Y. Ikeda, S. H. Sun, and E. E. Fullerton, J. Phys. D, 2002, 35(19): R157
75. D. Weller and A. Moser, IEEE Transactions on Magnetics, 1999, 35(6): 4423
76. O. A. Ivanov, L. V. Solina, V. A. Demshina, and L. M. Magat, Fizika Metallov I Metallovedenie, 1973, 35(1): 92
77. B. Zhang and W. A. Soffa, Scripta Metall Mater, 1994, 30(6): 683
78. S. I. Iwasaki, IEEE Transactions on Magnetics, 1984, 20(5): 657

79. E. J. Black, J. A. Bain, and T. E. Schlesinger, IEEE Transactions on Magnetics, 2007, 43(1): 62
80. R. E. Rottmayer, S. Batra, D. Buechel, W. A. Challener, J. Hohlfeld, Y. Kubota, L. Li, B. Lu, C. Mihalcea, K. Mountfield, K. Pelhos, C. B. Peng, T. Rausch, M. A. Seigler, D. Weller, and X. M. Yang, IEEE Transactions on Magnetics, 2006, 42(10): 2417
81. Y. Matsuura, J. Magn. Magn. Mater., 2006, 303(2): 344
82. J. Svoboda, Magnetic Techniques for the Treatment of Materials, Dordrecht, The Netherlands: Kluwer Academic Publishers, 2004
83. J. Fidler, D. Suess, and T. Schrefl, Rare-Earth Intermetallics for Permanent Magnet Applications, in Handbook of Magnetism and Advanced Magnetic Materials, Vol. 4: Novel Materials, edited by H. Kronmüller and S. Parkin, New York: John Wiley & Sons Inc., 2007
84. E. F. Kneller and R. Hawig, IEEE Transactions on Magnetics, 1991, 27(4): 3588
85. R. Skomski and J. M. D. Coey, Phys. Rev. B, 1993, 48(21): 15812
86. J. Li, Z. L. Wang, H. Zeng, S. H. Sun, and J. P. Liu, Appl. Phys. Lett., 2003, 82(21): 3743
87. H. Zeng, J. Li, Z. L. Wang, J. P. Liu, and S. H. Sun, Nano Lett., 2004, 4(1): 187
88. Y. L. Hou, S. H. Sun, C. B. Rong, and J. P. Liu, Appl. Phys. Lett., 2007, 91(15): 153117